THE JOURNAL OF BIOLOGICAL CHEMISTRY VOL. 286, NO. 6, pp. 4443–4453, February 11, 2011

14*S*,21*R*-Dihydroxydocosahexaenoic Acid Remedies Impaired Healing and Mesenchymal Stem Cell Functions in Diabetic Wounds*[S]

Received for publication, January 16, 2010, and in revised form, October 26, 2010 Published, JBC Papers in Press, November 26, 2010, DOI 10.1074/jbc.M110.100388

Haibin Tian, Yan Lu, Shraddha P. Shah, and Song Hong[1]

From the Center of Neuroscience Excellence, Louisiana State University Health Science Center, New Orleans, Louisiana 70112

Treatment of diabetes-impaired wound healing remains a major unresolved medical challenge. Here, we identified suppressed formation of a novel reparative lipid mediator 14*S*,21*R*-dihydroxydocosa-4*Z*,7*Z*,10*Z*,12*E*,16*Z*,19*Z*-hexaenoic acid (14*S*,21*R*-diHDHA) in cutaneous wounds of diabetic *db/db* mice. These results indicate that diabetes impedes the biosynthetic pathways of 14*S*,21*R*-diHDHA in skin wounds. Administration of exogenous 14*S*,21*R*-diHDHA to wounds in diabetic animals rescued healing and angiogenesis. When *db/db* mesenchymal stem cells (MSCs) were administered together with 14*S*,21*R*-diHDHA to wounds in diabetic animals, they coacted to accelerate wound re-epithelialization, granulation tissue formation, and synergistically improved vascularization. In the pivotal cellular processes of angiogenesis, 14*S*,21*R*-diHDHA enhanced VEGF release, vasculature formation, and migration of *db/db* dermal microvascular endothelial cells (DMVECs), as well as remedied paracrine angiogenic functions of *db/db* MSCs, including VEGF secretion and the promotion of DMVEC migration and vasculature formation. Our results show that 14*S*,21*R*-diHDHA activates the p38 MAPK pathway in wounds, *db/db* MSCs, and DMVECs. Overall, the impeded formation of 14*S*,21*R*-diHDHA described in this study suggests that diabetes could affect the generation of pro-healing lipid mediators in wound healing. By restoring wound healing and MSC functions, 14*S*,21*R*-diHDHA is a new lead for the development of better therapeutics used in treating wounds of diabetics.

Millions suffer from diabetes-impaired wound healing (1). Reports have documented that dysregulated cellular and molecular processes are responsible for this impairment in wound healing. Impaired vascularization or angiogenesis has been confirmed to be one of the most important etiologies for impaired healing of diabetic wounds (1, 2). Hence, rescuing impaired angiogenesis is a reasonable approach to enhance wound healing in diabetics (1).

Lipid-derived molecules also may play important roles as mediators in wound healing and angiogenesis. As shown from our lipidomic analysis, the essential fatty acid docosahexaenoic acid (DHA)[2] is a relatively abundant endogenous lipid component in blood and in wounded full-thickness skin. DHA ameliorates complications of diabetes (3) and significantly promotes wound healing (4). Resolvins, neuroprotectins/protectins, and maresins are lipid mediators (LMs) that are generated naturally from essential ω-3 fatty acids, DHA, and eicosapentaenoic acid, during acute inflammation and have potent anti-inflammatory functions (5–9). Their discovery established a new avenue toward unraveling the mechanisms behind the beneficial effects of DHA. Neuroprotectin/protectin D1 was found to enhance corneal wound healing (10). Recently, we identified 14*S*,21*R*-dihydroxydocosa-4*Z*,7*Z*,10*Z*,12*E*,16*Z*,19*Z*-hexaenoic acid (14*S*,21*R*-diHDHA), a novel endogenous lipid mediator derived from DHA, in skin wounds that is capable of promoting wound healing and angiogenesis (11).

However, diabetic hyperglycemia and the concomitant oxidative stress damage DNA, proteins, and lipids in various tissues resulting in dysfunction of cells and enzyme systems involved in wound healing and LM biosynthesis (12–15). Therefore, diabetic complications are likely to dysregulate the biosynthesis of DHA-derived LMs in wound healing. Treatments that counteract this dysregulation may improve diabetic wound healing.

Recent studies have used bone marrow-derived mesenchymal stem cells (MSCs) to promote wound healing (16–18). MSC transplants promote wound healing and angiogenesis by producing paracrine angiogenic cytokines (2, 19–21) and by possibly differentiating into skin cells (2, 19–24). Treating diabetics with their own MSCs can avoid side effects, including a graft *versus* host response associated with nonautologous transplantation. However, diabetes also impairs MSC pro-healing functions (24).

To date there are no reports regarding LM formation or the effects of LM either in diabetic wound healing and angiogenesis or in diabetes-impaired MSC functions. To identify dys-

* This work was supported by National Institutes of Health Grant 1R01DK087800 (to S. H.) and by the Start-up Fund from the Neuroscience Center of Excellence, LSUHSC-NO (to S. H.).

[S] The on-line version of this article (available at http://www.jbc.org) contains supplemental Figs. S1–S6.

[1] To whom correspondence should be addressed: Center of Neuroscience Excellence, Louisiana State University Health Sciences Center, Lions Bldg., 2020 Gravier St., Ste. D, New Orleans, LA 70112. Tel.: 504-599-0838; Fax: 504-599-0891; E-mail: shong@lsuhsc.edu.

[2] The abbreviations used are: DHA, docosahexaenoic acid; MSC, mesenchymal stem cell; 14*S*,21*R*-diHDHA, 14*S*,21*R*-dihydroxydocosa-4*Z*,7*Z*,10*Z*,12*E*,16*Z*,19*Z*-hexaenoic acid; DMVEC, dermal microvascular endothelial cell; LM, lipid mediator; HETE, hydroxyeicosatetraenoic acid; LOX, lipoxygenase; LC-UV-MS/MS, liquid chromatography-ultraviolet detector-linear ion trap mass spectrometer; P, platelet; h-P450, human-P450.

regulation in the formation of DHA-derived LMs in diabetic mice, we have conducted LC-MS/MS-based lipidomic studies (25) of wounded skin from diabetic *db/db* and nondiabetic *db/+* mice. Here, we describe the identification of a novel DHA-derived mediator 14*S*,21*R*-diHDHA, which is suppressed in wounds of diabetic *db/db* mice and 12/15(or L-12)-lipoxygenase gene knock-out mice (12/15-LOX is most related to human 15-LOX type-1) (26). We demonstrate that 14*S*,21*R*-diHDHA restored wound healing and angiogenesis in diabetic mice as well as the pro-healing functions of *db/db* MSCs and key cellular processes of angiogenesis. It activates the p38 MAPK but does not affect the ERK1/2, although signaling through both p38 MAPK and ERK1/2 is critical for wound healing and associated angiogenesis (27, 28).

EXPERIMENTAL PROCEDURES

Studies were blinded. Animal protocols were approved by the Institutional Animal Care and Use Committee and Institutional Review Board of Louisiana State University Health Sciences Center, New Orleans.

Mice—Diabetic *db/db* (BKS.Cg-m+/+leprdb/J) and nondiabetic *db/+* mice (10-week-old, female) (Jackson Laboratory, Bar Harbor, ME) were used when blood glucose was 22–35 mM for *db/db* mice and 5–10 mM for *db/+* mice, as measured by a glucometer. 12/15-LOX (Alox15) or L-12-LOX gene knock-out (12/15-LOX-KO) and C57Bl/6J congenic control mice (10 weeks, female) were purchased from The Jackson Laboratory. The KO mice do not express the 12/15-(or L-12)LOX and have a C57BL/6J genetic background (29–32).

Isolation and Identification of DMVECs from db/db and db/+ Mice—This was done as described previously (33) and as detailed in supplemental Fig. S1. The final DMVECs were 95% $CD31^+$ and VE-$cadherin^+$. The cellular identity of the DMVECs was confirmed by immunocytochemical analysis, which demonstrated their purity and expression of the endothelial markers CD31, VE-cadherin, von Willebrand factor, and Tie-2 (supplemental Fig. S1*A*).

Isolation and Identification of MSCs from Mice—MSCs were isolated as published previously (22) and described in supplemental Fig. S1. To verify the identity of the MSCs, we first confirmed their differentiation ability according to a previous report (18). The isolated MSCs exhibited a spindle-shaped morphology (supplemental Fig. S1*Bi*). After culturing the MSCs for 10 days in osteogenic or adipocytic differentiation media, the cells differentiated into the osteoblastic (supplemental Fig. S1*Bii*) or adipocytic lineages (supplemental Fig. S1*Biii*), respectively. We also analyzed the MSCs by flow cytometry as in Ref. 18 and confirmed that more than 95% of cells expressed MSC marker Sca-1 (supplemental Fig. S1*Biv*) (18, 19, 22).

Splinted Excisional Wound Healing Model—This model was established as described previously (34) with minor modification. Briefly, paired 5-mm circular, full-thickness wounds were made symmetrically along the midline on the dorsal skin of mice. For each wound on a diabetic *db/db* mouse, 14*S*,21*R*-diHDHA in DMEM (50 ng/wound), MSCs (*db/db* or *db/+*, 10^6 cells/wound), or 14*S*,21*R*-diHDHA (50 ng) plus MSCs (*db/db,* 10^6 cells) was applied to the wound bed (10 μl) and injected intradermally at four points (10 μl/site) distributed evenly near the wound edge (50 μl total/wound). A donut-shaped silicone splint was adhered around the wound to prevent skin contraction and to allow wounds to heal through re-epithelialization and granulation (34). This model closely parallels human wound healing (34). In another experiment, wounds were imposed to the skin of *db/+* mice, and 14*S*,21*R*-diHDHA in DMEM (50 ng/wound), MSCs (*db/+*, 10^6 cells/wound), or 14*S*,21*R*-diHDHA (50 ng) plus MSCs (*db/+*, 10^6 cells) was applied to the wound bed and wound edge. Skin wounds were also generated in 12/15-LOX-KO and control C57/6J mice and collected for the analysis of lipids.

Sample Preparation and LC-UV-MS/MS Analysis of Lipid Mediators—Prostaglandin $F_{2\alpha}$-d_4, DHA, DHA-d_5, 5*S*,6*R*-dihydroxyeicosatetraenoic acid (HETE), 5*S*,6*S*-diHETE, and porcine L-12-LOX were supplied by Cayman Chemicals (Ann Arbor, MI). Neuroprotectin-D1/protectin-D1/(NPD1/PD1) and its isomers prepared by total organic synthesis were provided by Dr. Nicolas G. Bazan, Neuroscience Center of Excellence, Louisiana State University Health Sciences Center, and by Dr. Charles N. Serhan, Brigham and Women's Hospital, Harvard Medical School. Adam's catalyst (PtO_2) was from Sigma.

Lipid samples and standards were handled under dimmed light, stored in −80 °C freezer with head space of the containing vials purged by argon gas, and sealed tightly. The aqueous solutions of DHA and DHA derivatives were freshly prepared on water-ice and used right away. Wounded skin was collected immediately after the mice were sacrificed, soaked in ice-cold acetone, chilled immediately with liquid nitrogen, and stored in −80 °C freezer. Within 12 h of storage at −80 °C after collection, each tissue sample was extracted with ice-cold methanol three times by homogenization and sonication on ice. The acetone and methanol for the extraction contained 0.1% butylated hydroxytoluene to suppress auto-oxidation. The extracts for each sample were pooled together and purified via C18 solid-phase extraction and then analyzed using a LC-UV-MS/MS (LTQ, Thermo, Waltham, MA). The deuterated internal standards added to samples at the time of collection for quantification of interested components were prostaglandin $F_{2\alpha}$-d_4 (20 ng), 14*S*,21*R*-diHDHA-d_4 (10 ng), 14*S*-HDHA-d_5 (10 ng), and DHA-d_5 (20 ng) (35–38). The LC unit was equipped with a chiral column (ChiralPak-IA, 150 × 2.1 mm × 5 μm) (Chiral Technologies, West Chester, PA). The mobile phase had a flow rate of 0.2 ml/min, eluted as B (methanol/H_2O/acetic acid = 27:73:0.01) from 0 to 1 min, ramped from B/methanol (40:60) to B/methanol (20:80) by 50 min, then ramped to methanol by 55 min, and kept as methanol. DHA, DHA-d_5, 14*S*-HDHA, 14*S*-HDHA-d_5, 14*S*,21*R*-diHDHA, or 14*S*,21*R*-diHDHA-d_4 from the effluent of the chiral LC coupled to the mass spectrometer was analyzed on the basis of selected MS/MS ion chromatograms at mass to charge ratio (*m/z*) 191 of MS/MS 327, *m/z* 196 of MS/MS 332, *m/z* 205 of MS/MS 343, *m/z* 205 of MS/MS 348, *m/z* 253 of MS/MS 359, or *m/z* 253 of MS/MS 363, respectively. The amount of DHA, 14*S*-HDHA, or 14*S*,21*R*-diHDHA in each sample was then quantified based on its LC peak area ratio relative to that of its deuterated internal standard DHA-d_5, 14*S*-HDHA-d_5, or 14*S*,21*R*-diHDHA-d_4, respectively (39).

14*S*,21*R*-diHDHA and 14*S*,21*S*-diHDHA were generated by incubating 14*S*-hydroxy-DHA (14*S*-HDHA) (50 μg) with 1 nmol of human cytochrome P450 mixture (h-P450) (BioCatalytics, Pasadena, CA) at 30 °C for 12 h. Under the same condition, 14*R*,21*R*-diHDHA and 14*R*,21*S*-diHDHA were generated from 14*R*-HDHA by the h-P450 (11). The h-P450 contains NADPH cofactor, buffer salts, and h-P450 (recombinant human CYP1A2, -2C8, -2C9, -2D6, -2E1, and -3A4) in the company's proprietary ratios. 14*S*-HDHA and 14*S*-HDHA-d_5 were prepared by incubating DHA and DHA-d_5 (50 μg/each), respectively, with porcine L-12-LOX (1000 units) in buffer containing 0.1 M Tris at pH 7.4 and 0.01% Triton X-114 at 37 °C for 20 min. At the end of the incubation, 3 mg of $NaBH_4$ was added (5, 11). Additionally 14*S*-HDHA and 14*R*-HDHA were prepared from racemic 14*S/R*-HDHAs (Cayman Chemicals) by a ChiralPak-AD-RH LC chiral column (150 × 2.1 mm × 5 μm) (Chiral Technologies) (40). The mobile phase had a flow ate of 0.15 ml/min, eluted as D (acetonitrile/H_2O/acetic acid = 45:55:0.01) from 0 to 45 min, ramped to acetonitrile from 45.1 to 60 min, returned to acetonitrile flow for 10 min, and then run as D again for 10 min (11). 14*S*,21*R*-diHDHA-d_4 was prepared by the incubation of 14*S*-HDHA-d_5 with human P450 (11). Only the DHA and 14*S*-HDHA with not less than 98% purity (without detectable oxidation artifacts), analyzed by chiral LC-UV-MS/MS above, were used to prepare 14*S*-HDHA and 14*S*,21*R*-diHDHA, respectively.

The incubations were extracted three times with 2 volumes of ethyl acetate after its pH was adjusted to 3.5–4. The extracts were washed with 2 volumes of LC-MS-grade water twice and then reconstituted with methanol. Products in the incubations were isolated by the chiral LC-UV-MS/MS as above (supplemental Fig. S3) (11). The fraction of 14*S*,21*R*-diHDHA was dried completely by N_2 gas blower and reconstituted to ethanol. The purified 14*S*,21*R*-diHDHA and 14*S*,21*R*-diHDHA-d_4 were quantified by LC-UV-MS/MS using NPD1 (10,17-diHDHA, 99% purity) (38) as an internal standard. Additionally, the purified 14*S*-HDHA-d_5 was quantified by LC-UV-MS/MS using ±14-HDHA (Cayman Chemical) as the standard. The 14*S*,21*R*-diHDHA preparation was found to be of ~96% purity calculated from the LC-UV at 235 nm (supplemental Fig. S2, *A* and *B*) using above ChiralPak-IA-based chiral LC-UV-MS/MS. This is consistent with the UV spectrum with a singlet band of 235 nm maximum absorbance wavelength, which was acquired from LC-UV (supplemental Fig. S2*C*), and stand-alone DU-800 UV/visible spectrophotometer (Beckman Coulter, Brea, CA) (supplemental Fig. S2*D*). Six carbon-carbon double bonds hydrogenated 14*S*,21*R*-diHDHA (H_{12}-14*S*,21*R*-diHDHA) was generated by bubbling hydrogen gas through a methanol solution of 14*S*,21*R*-diHDHA, in which Adam's catalyst PtO_2 (~1 mg) was suspended (20 min, room temperature) (41–43).

Analysis of Wound Healing—Wounds rimmed with 2 mm of normal skin were excised from *db/db* mice sacrificed at day 8 post-wounding and *db/+* mice at day 5 post-wounding, fixed, and embedded (34). Cryosections (10 μm thick/section) of wounds were analyzed to determine relative epithelial gap (recorded as a percent relative to that of the initial wound) and granulation tissue area after hematoxylin and eosin (H&E) staining. Results were expressed as decreased percentage of relative epithelial gap compared with control ((relative epithelial gap in control − relative epithelial gap in treatment)/relative epithelial gap in control × 100%) and increased percentage of granulation tissue area compared with control ((granulation tissue area in treatment − granulation tissue area in control)/granulation tissue area in control × 100%). Wound vascularity, as determined by CD31 − positive area per field/total wound bed area per field × 100% (% vascularity), was assessed by staining vessel endothelial cells with monoclonal rat anti-mouse CD31 antibody (BD Biosciences) followed by anti-rat IgG horseradish peroxidase (HRP) detection kits (BD Biosciences) and then by hematoxylin for nuclei. Images were captured using a microscope. Results are depicted as increased percentage of wound vascularity compared with control ((% vascularity in treatment − % vascularity in control)/% vascularity in control × 100%).

Preparation of MSC-conditioned Media—Quiescent *db/db* MSCs (3×10^5 cells) were prepared by starvation in DMEM containing high glucose (25 mM) and 0.5% FBS (Invitrogen) for 12 h. The cells were then cultured in DMEM containing high glucose (25 mM) without or with 14*S*,21*R*-diHDHA (100 nM) for 24 h. MSCs from nondiabetic *db/+* mice were cultured similarly in the absence of 14*S*,21*R*-diHDHA. After centrifugation at 3,000 × *g* for 15 min at 4 °C, the supernatant became "MSC-conditioned medium."

DMVEC Migration—Quiescent *db/db* and *db/+* DMVECs at 80% confluence were resuspended in DMEM containing 25 mM (for *db/db* cells) or 5 mM (for *db/+* cells) glucose and added to the upper chamber of a 24-transwell plate (8-μm pore, BD Biosciences) at 1×10^5 cells/well. DMEM containing high glucose (25 mM) or low glucose (5 mM) in the presence or absence of 14*S*,21*R*-diHDHA (100 nM) or MSC-conditioned media were added to the lower chamber. The cells were allowed to migrate for 4 h at 37 °C in 5% CO_2. Migrated cells, which were attached to the undersides of membranes, were stained with Giemsa. The images were captured by a microscope. Results were expressed as increased percentage of migrated DMVECs compared with control using the equation ((migrated DMVECs per field in treatment − migrated DMVECs per field in control)/migrated DMVECs per field in control × 100%).

DMVEC Vasculature Formation—Quiescent *db/db* and *db/+* DMVECs were cultured on Matrigel (BD Biosciences) in DMEM containing high glucose (25 mM, for *db/db* cells) or low glucose (5 mM, for *db/+* cells) in the presence or absence of 14*S*,21*R*-diHDHA (100 nM) or MSC-conditioned media for 24 h at 37 °C in 5% CO_2. The vasculature length was measured using a microscope and ImageJ1.40 software (National Institutes of Health). Results were expressed as increased percentage of vasculature length compared with control using the equation ((vasculature length per field in treatment − vasculature length per field in control)/vasculature length per field in control × 100%).

Bio-Plex Protein Array—Quiescent *db/db* DMVECs (3×10^5 cells) were cultured in DMEM containing high glucose (25 mM) in the presence or absence of 14*S*,21*R*-diHDHA for

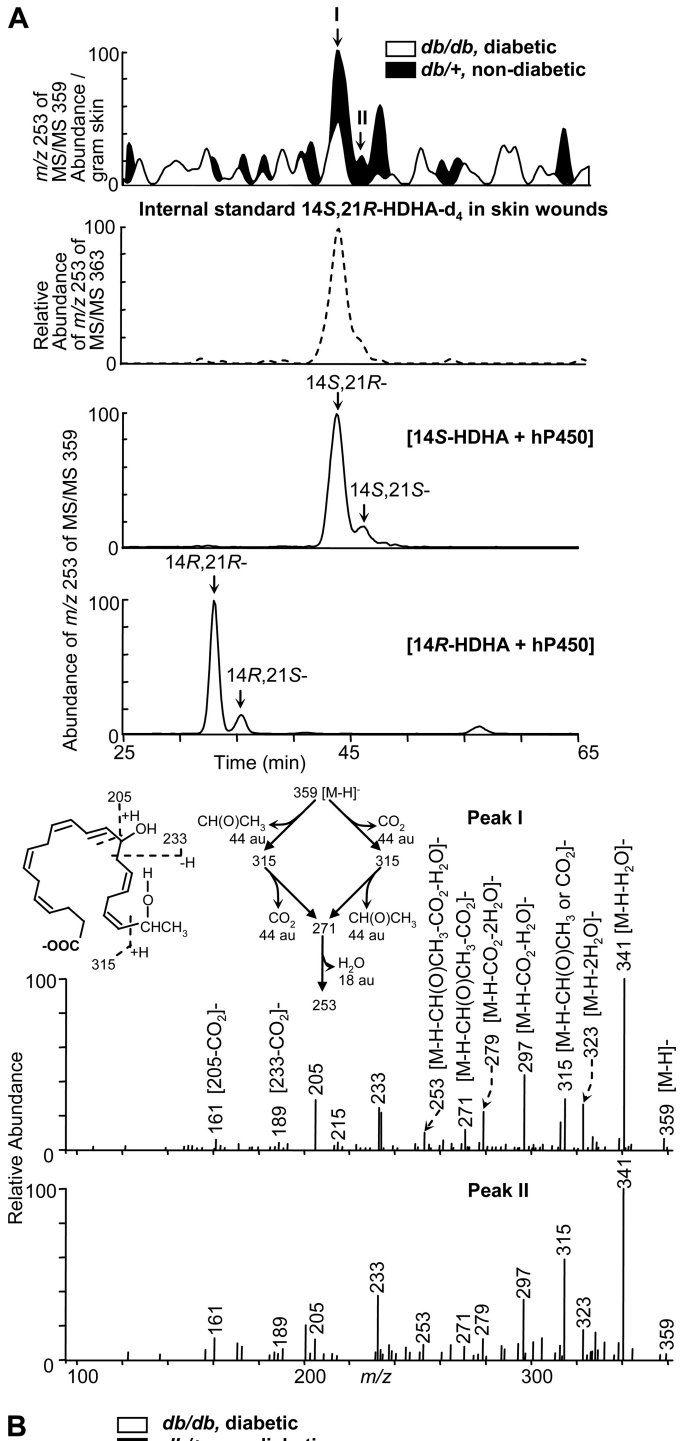

FIGURE 1. **Formation of 14*S*,21*R*-diHDHA was suppressed in skin wounds in diabetic *db/db* mice compared with nondiabetic *db*/+ mice.** Wounded skin was harvested from mice immediately following sacrifice at day 1 after the splinted excisional wounding was performed. *A,* overlay ChiralPak-IA-based chiral LC-MS/MS chromatograms (*top panels*) of wounds of *db*/+ (*solid black*) and *db/db* (*open line*) mice, and spectra (nonwide band) (*bottom two panels*) of peak I and peak II found in wounds of *db*/+ mice. For comparison, the ion abundance of each selected MS/MS ion chromatogram was divided by the extraction recovery of the stable deuterated internal standard 14*S*,21*R*-diHDHA-d_4 added to the sample and then normalized per g of skin. The *2nd panel* is a selected ion chromatogram at *m/z* 253 of MS/MS 363 for internal standard 14*S*,21*R*-diHDHA-d_4 added to and extracted from skin wounds. This deuterated compound was added to skin wounds collected from mice and used as the internal standard for the quantification of 14*S*,21*R*-diHDHA (see details under "Experimental Procedures"). Chromatograms of 14*S*,21*R*-diHDHA and 14*S*,21*S*-diHDHA (generated from 14*S*-HDHA by h-P450) as well as 14*R*,21*S*-diHDHA and 14*R*,21*R*-diHDHA (generated from 14*R*-HDHA by h-P450) are shown in the *3rd* and *4th panels*, respectively. *B,* quantification of 14*S*,21*R*-diHDHA, 14*S*-HDHA, and DHA in wounds of *db*/+ (*solid black*), *db/db* (*open bar*), 12/15-LOX-knock-out mice (*light gray*), and C57BL/6J mice (*dark gray*) via ChiralPak-IA-based chiral LC-MS/MS using stable deuterated internal standards. Results are mean ± S.E. ($n = 3$). *, $p < 0.05$ compared with control.

24 h. The supernatants were collected. VEGF in *db/db* DMVEC supernatants or MSC-conditioned media was quantified by the Bio-Plex Protein array kit (Bio-Rad).

Western Blot—14*S*,21*R*-diHDHA (50 ng/wound) was immediately injected into wound bed and edge in *db*/+ and *db/db* mice after wounds were made. 15 min later, wounds were collected for analysis of expressions of P-p38 and p38. Quiescent *db/db* DMVECs or *db/db* MSCs were incubated in DMEM with or without 14*S*,21*R*-diHDHA (100 nM) for 10–120 min. Cells were lysed for analysis of expression of P-p38 and P-ERK1/2 (phosphorylated forms) as well as p38 and ERK1 (nonphosphorylated forms). Western blot was performed as described previously (27, 28) with minor modification. Briefly, 30 μg of total proteins from each lysed sample was resolved by SDS-PAGE on 4–15% Tris-HCl gels (Bio-Rad). The electrotransferred protein bands were stained by primary antibodies for P-p38 or P-ERK1/2 (BD Biosciences), followed by fluorescent-labeled secondary antibodies (LI-COR, Lincoln, NB), and finally quantified using an Odyssey Imaging System (LI-COR). When necessary, blots were stripped and reprobed.

Statistical Analysis—Results were analyzed by one-way ANOVA analysis of variance followed by Fisher's LSD post hoc comparison and expressed as means ± S.E. A value of $p < 0.05$ was considered significant.

RESULTS

Suppressed Formation of 14S,21R-diHDHA in Skin Wounds of Diabetic Mice—To determine whether diabetes dysregulates DHA-derived LM formation in skin wounds, we first conducted LC-UV-MS/MS based mediator-lipidomic studies of wounded skin from diabetic *db/db* and nondiabetic *db*/+ mice. Two diHDHA chromatographic peaks (I and II) of ion *m/z* 253 from MS/MS *m/z* 359 were reduced in wounds of diabetic *db/db* mice compared with those of nondiabetic *db*/+ mice (Fig. 1*A*). The full-scan MS/MS spectra of peaks I and II (Fig. 1*A*) possessed ions at *m/z* 359 $[M - H]^-$, 341 $[M - H\text{-}H_2O]^-$, 323 $[M - H\text{-}2H_2O]^-$, 297 $[M - H\text{-}CO_2\text{-}H_2O]^-$, and 279 $[M - H\text{-}CO_2\text{-}2H_2O]^-$ that were consistent with the molecular weight of 360, one carboxyl (for loss of one CO_2 (44 atomic units)), and two hydroxyls (for $2H_2O$ loss);

ions *m/z* 205, 233, 189 [233 − CO_2]$^-$, and 161 [205 − CO_2]$^-$ indicated a hydroxyl at C14. Another hydroxyl at the C21 position was indicated by ions *m/z* 315 [M − H-CH(O)CH_3]$^-$, 271 [M − H-CO_2-CH(O)CH_3]$^-$, and 253 [M − H-H_2O-CO_2-CH(O)CH_3]$^-$ that involved C20-C21 cleavage in molecular ion *m/z* 359[M − H]$^-$ and loss of CH(O)CH_3 (44 atomic units) derived from "−H(OH)C21-H_3C22 terminal" group of the molecular ion *m/z* 359[M − H]$^-$ (*insets, 5th panel* of Fig. 1*A*). Additionally, ion *m/z* 315 could be [M − H-CO_2]$^-$, which was generated by losing CO_2 (44 atomic units) from molecular ion *m/z* 359 [M − H]$^-$; and it further transformed to *m/z* 271 [M − H-CO_2-CH(O)CH_3]$^-$ and 253 [M − H-H_2O-CO_2-CH(O)CH_3]$^-$ by the cleavage equivalent to what occurred in the formation of *m/z* 315 [M − H-CH(O)CH_3]$^-$ from molecular ion *m/z* 359 [M − H]$^-$ and the loss of CH(O)CH_3 (see MS/MS fragmentation pathways in insets of the *5th panel* of Fig. 1*A*). As an α-cleavage to 21-hydroxyl, C20-C21 cleavage generated MS/MS ions *m/z* 271 [M − H-CO_2-CH(O)CH_3]$^-$ and 253 [M − H-H_2O-CO_2-CH(O)CH_3]$^-$ that are the fingerprints showing 21-hydroxyl in diHDHAs. In brief, these structural diagnostic ions indicate that peaks I and II are 14,21-diHDHA (Fig. 1*A*), namely 14,21-diHDHAs existed in wounds (Fig. 1*A, top*).

The LC-MS/MS spectrum of H_{12}-14*S*,21*R*-diHDHA prepared from hydrogenation of 14*S*,21*R*-diHDHA showed molecular ion *m/z* 371 [M − H] and ions *m/z* 353 [M − H-H_2O]$^-$ and 335 [M − H-2H_2O]$^-$; the 14-hydroxyl was demonstrated by MS/MS ions *m/z* 157, 211, and 197 [241-CO_2]$^-$; The 21-hydroxyl was demonstrated by *m/z* 325, 323 [325–2H], 307 [325-H_2O]$^-$, and 281 [325-CO_2]$^-$. These data are consistent with the structure of H_{12}-14*S*,21*R*-diHDHA, consequently support the 14,21-diHDHA structure (supplemental Fig. S2*E*). The ChiralPak-IA-based LC condition above is able to separate chromatographically four 14,21-diHDHA diastereomers, including 14*S*,21*R*-diHDHA and 14*S*,21*S*-diHDHA generated from 14*S*-HDHA by P450 (Fig. 1*A*, *3rd panel*); and 14*R*,21*R*-diHDHA and 14*R*,21*S*-diHDHA generated from 14*R*-diHDHA by P450 (Fig. 1*A*, *4th panel*); as well as an enantiomic pair of 14*S*-HDHA and 14*R*-HDHA. The order of elution for 14,21-diHDHAs is based on the following observations: diastereomer 5*S*,6*R*-dihydroxyeicosatetraenoic acid (HETE) eluted before 5*S*,6*S*-diHETE with same double bond geometry; diastereomer 10*R*,17*S*-dihydroxy-NPD1 eluted before 10*S*,17*R*-dihydroxy-NPD1; and 10*S*,17*R*-dihydroxy-NPD1 eluted before 10*S*,17*S*-dihydroxy-NPD1 (the structures of NPD1 or PD1 stereoisomers were already elucidated and presented by Serhan *et al.* (44)) (supplemental Fig. S2*F*). The elution order is from 14*R*,21*R*-diHDHA (the earliest), 14*R*,21*S*-diHDHA, 14*S*,21*R*-diHDHA, to 14*S*,21*S*-diHDHA (the latest), which is the same as that for ChiralPak-AD-RH LC chiral column (11) except that 14*R*,21*S*-diHDHA and 14*S*,21*R*-diHDHA overlapped for the latter. The MS/MS spectra and chiral LC retention times for peaks I and II of wound tissue matched those for 14*S*,21*R*-diHDHA and 14*S*,21*S*-diHDHA, respectively, generated from 14*S*-hydroxy-DHA by P450 enzyme (Fig. 1*A*) (11). Therefore, peaks I and II from wounds are 14*S*,21*R*-diHDHA and 14*S*,21*S*-diHDHA. Their amount ratio was 9.5:1 based on their peak areas of the selected ion chromatogram at *m/z* 359 for wounds of nondiabetic mice.

The formation of 14*S*,21*R*-diHDHA and its biosynthetic precursor 14*S*-HDHA (11) was reduced, although the reduction of 14*S*-HDHA was modest, and 14*S*,21*S*-diHDHA was under the detection limit in wounds of diabetic mice compared with nondiabetic control animals (Fig. 1, *A* and *B*) based on LC-MS/MS quantification using deuterated internal standard of each compound. The DHA level was slightly reduced, but it was not significant. We also analyzed the skin wounds of 12/15-LOX-KO mice and controls. It was observed that the formation of 14*S*-HDHA was significantly reduced, and 14*S*,21*R*-diHDHA was found in the wounds of wild-type controls but was undetectable in the 12/15-LOX-KO mice, although DHA levels were not significantly different (Fig. 1*B, right panel*). This implicates that 12/15-LOX participates in the formation of 14*S*,21*R*-diHDHA and 14*S*-HDHA.

14S,21R-diHDHA Remedies Diabetic Wound Healing and Vascularization—Because 14*S*,21*R*-diHDHA formation was decreased in diabetic wounds, we were motivated to study whether administration of exogenous of 14*S*,21*R*-diHDHA could enhance wound healing. 14*S*,21*R*-diHDHA was applied into the wounds of *db/db* mice. Interestingly, the administration of 14*S*,21*R*-diHDHA promoted wound healing significantly (Fig. 2). In comparison with vehicle control, 14*S*,21*R*-diHDHA accelerated re-epithelialization and promoted granulation formation. Analysis of hematoxylin and eosin-stained cryosections of wounds collected at day 8 post-wounding revealed that the relative epithelial gap was decreased 36.2% (Fig. 2*B*, *left panel*), whereas the granulation tissue area was increased 60.7% (Fig. 2*B*, *right panel*). Because impaired vascularization or angiogenesis is a critical hallmark of nonhealing wounds in diabetes (45, 46), we investigated whether 14*S*,21*R*-diHDHA could promote vascularization during wound healing in diabetic mice. The data demonstrate that wounds from *db/db* mice treated with 14*S*,21*R*-diHDHA exhibited a 41.9% increase in vascularity compared with control animals at day 8 post-wounding (Fig. 2*C*). When 14*S*,21*R*-diHDHA was applied on wounds of *db/+* mice, the same effects on re-epithelialization, granulation formation, and vascularization were observed (supplemental Figs. S4 and S5).

We further used *in vitro* models of DMVEC migration and vasculature formation to investigate the action of 14*S*,21*R*-diHDHA on the cellular processes of angiogenesis. In simulated diabetic hyperglycemia (25 mM glucose in medium) (45, 46), 14*S*,21*R*-diHDHA promoted the cellular processes of angiogenesis through significantly enhancing *db/db* DMVEC migration 45.5% (Fig. 3*A*) and vasculature formation 40.8% (Fig. 3*B*). Moreover, diabetic *db/db* DMVECs treated with 14*S*,21*R*-diHDHA produced more vascular endothelial growth factor (VEGF), a potent angiogenic factor (47, 48), than control-treated cells (Fig. 3*C*). We also compared migration and vasculature formation between *db/db* DMVECs and *db/+* DMVECs and found *db/+* DMVECs could form a longer tube than *db/db* DMVECs without any treatment, but no difference was observed for migration. In addition, 14*S*,21*R*-diHDHA could also promote *db/+* DMVEC migration and vasculature formation (supplemental Fig. S6).

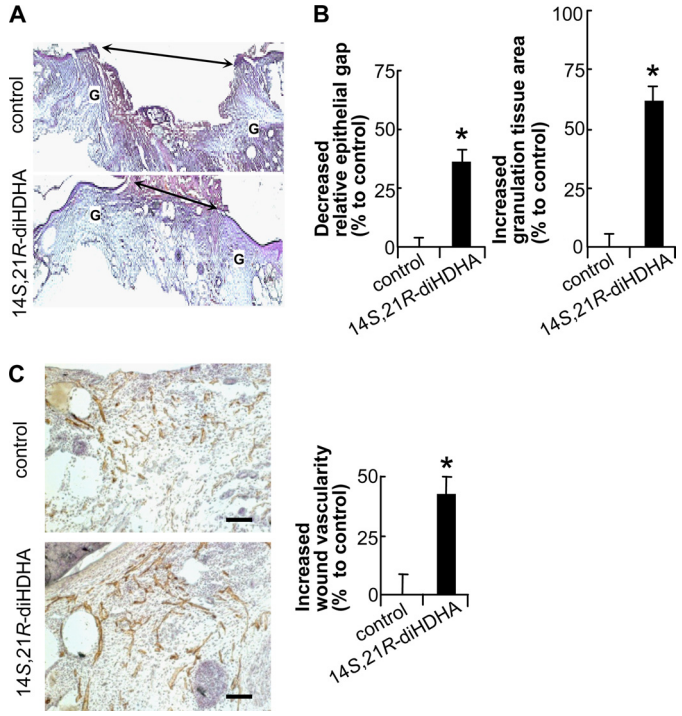

FIGURE 2. **14*S*,21*R*-diHDHA remedied impaired wound healing and vascularization in diabetic mice.** Splinted excisional wounding was conducted in *db/db* mice as in Fig. 1, followed by administration of 14*S*,21*R*-diHDHA to wounds (50 ng/wound). *A,* micrographs; *B,* quantitative analysis of H&E-stained cryosections of wounds show that 14*S*,21*R*-diHDHA treatment enhanced re-epithelialization and granulation tissue formation compared with the DMEM control, a decreased percentage of relative epithelial gap (*left panel*) and increased percentage of granulation tissue area (*right panel*) were observed ($n = 6$). *G,* granulation tissue; *double arrow,* epithelial gap. The control had a relative epithelial gap of 64.9 ± 2.0% and total granulation tissue area of 4250.0 ± 176.9 pixels/cryosection. *C,* 14*S*,21*R*-diHDHA increased wound vascularity. Micrographs (*left panel*) showing $CD31^+$ vessels and hematoxylin-stained nuclei in wound cryosections. The increased percentage of wound vascularity is presented on the *right* ($n = 12$). The wound vascularity of control animals was 4.4 ± 0.4%. *Scale bar,* 100 μm. Results are means ± S.E. *, $p < 0.05$ compared with control.

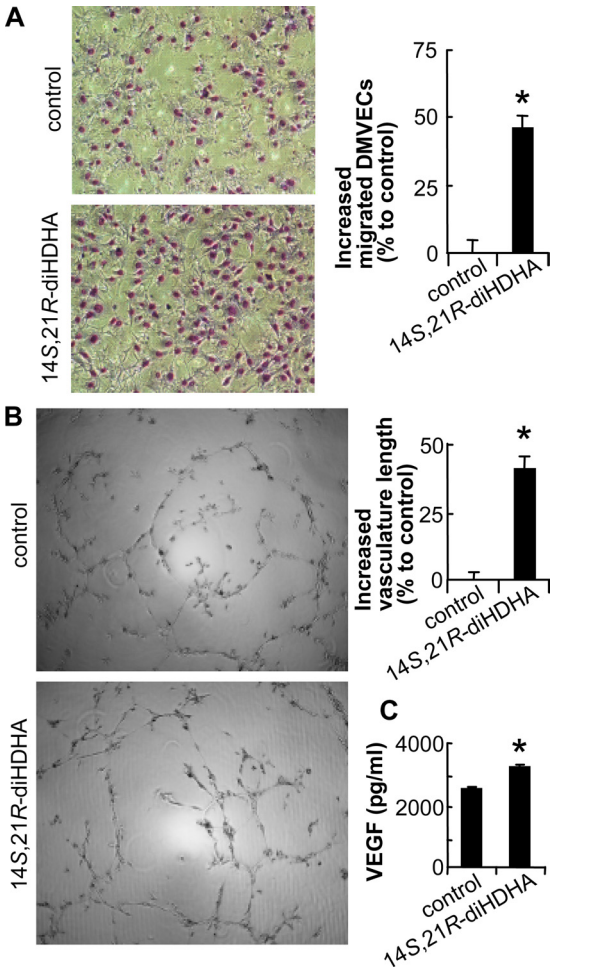

FIGURE 3. **14*S*,21*R*-diHDHA improved the cellular processes of angiogenesis in *db/db* DMVECs.** The cellular angiogenic processes of migration (*A*), vasculature formation (*B*), and VEGF release (*C*) were assayed *in vitro* using *db/db* DMVECs cultured under simulated hyperglycemic conditions (25 mM glucose) in the presence and absence (control) of 14*S*,21*R*-diHDHA (100 nM). Migration and vasculature formation are presented as increased percentages of migrated DMVECs per field ($n = 15$) and of vasculature length per field ($n = 4$), respectively, compared with control (migrated DMVECs, 118.0 ± 2.8 cells/field; vasculature length, 7.2 ± 0.3 mm/field). Representative images (*left panel*) and the quantification (*right panel*) are presented. VEGF secreted from DMVECs was measured using the Bio-Plex protein array ($n = 3$). Results are means ± S.E. *, $p < 0.05$ compared with control.

14S,21R-diHDHA Acts Together with db/db MSCs to Promote Wound Healing—Previous reports have demonstrated that MSCs from diabetic donors are less efficient at promoting wound healing (2). To determine whether 14*S*,21*R*-diHDHA and *db/db* MSCs together could enhance wound healing in *db/db* mice better than either one alone, we administered 14*S*,21*R*-diHDHA (50 ng/wound) along with *db/db* MSC transplantation (10^6 cells/wound). This treatment resulted in a decrease in the relative epithelial gap of 75.2% (Fig. 4, *A* and *B*) and an increase in granulation tissue area of 107.8% (Fig. 4, *A* and *C*) at day 8 post-wounding. In particular, 14*S*,21*R*-diHDHA combined with *db/db* MSCs was more effective than *db/db* MSCs alone (Fig. 4, *A*–*C*) or 14*S*,21*R*-diHDHA alone (Fig. 2, *A* and *B*) in accelerating wound healing. In addition, administration of 14*S*,21*R*-diHDHA with *db/db* MSCs was as effective as *db/+* MSCs alone (Fig. 4, *A*–*C*). Treatment with *db/db* and *db/+* MSCs promoted re-epithelialization with decreased percentages of the relative epithelial gap of 25.6 and 61.7%, respectively, as well as increased percentages of the total granulation area by 52.0 and 82.4%, respectively, compared with control (Fig. 4, *A*–*C*). Indeed, *db/db* diabetic MSCs are less efficient than *db/+* nondiabetic MSCs in promoting wound healing, indicating impaired wound healing due to diabetes. Therefore, 14*S*,21*R*-diHDHA coacts with *db/db* MSCs to promote diabetic wound healing and compensates for the diabetes-impaired pro-healing functions of *db/db* MSCs. In addition, we also confirmed that 14*S*,21*R*-diHDHA coacts with *db/+* MSCs to promote wound healing on *db/+* mice (supplemental Fig. S4).

14S,21R-diHDHA Remedies Diabetes-impaired Functions of db/db MSCs and Acts Synergistically with db/db MSCs in Promoting Angiogenesis—We further investigated whether 14*S*,21*R*-diHDHA would improve the function of *db/db* MSCs in promoting diabetes-impaired angiogenesis. The angiogenic functions of *db/db* MSCs were impaired compared with *db/+* MSCs even though *db/db* MSCs increased wound vascularity 78.5% (*versus* 130.1% for *db/+* MSCs) relative to

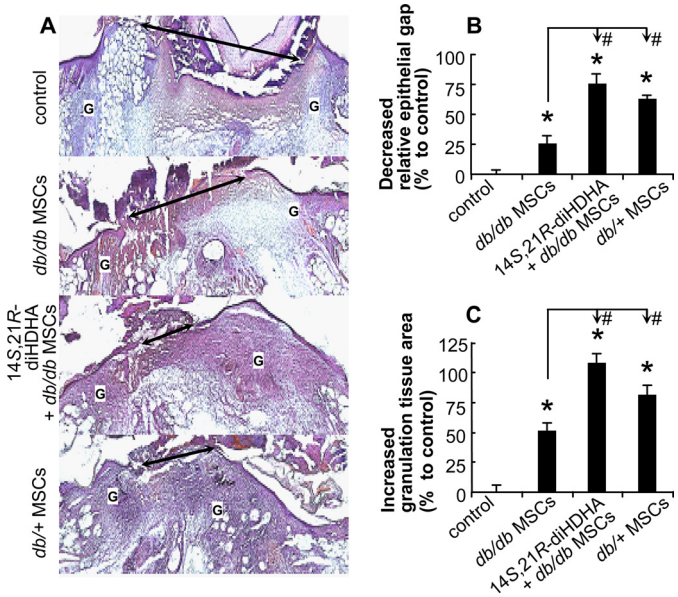

FIGURE 4. **14*S*,21*R*-diHDHA acted together with *db/db* MSCs to promote wound healing.** Splinted excisional wounding was conducted in *db/db* mice as in Fig. 1, followed by treatment of the wounds with vehicle, *db/db* MSCs, *db/db* MSCs plus 14*S*,21*R*-diHDHA, or *db*/+ MSCs alone (14*S*,21*R*-diHDHA, 50 ng/wound; MSCs, 10^6 cells/wound). Wounds were collected from *db/db* mice at day 8 post-wounding. *A,* representative micrographs of H&E-stained cryosections of wounds. *Double arrow,* epithelial gap; *G,* granulation tissue. *B,* decreased percentage of the relative epithelial gap; *C,* increased percentage of the granulation tissue area as compared with controls that had a relative epithelial gap of 64.9 ± 2.0% and total granulation tissue area of 4250.0 ± 176.9 pixels/cryosection. Results are means ± S.E. ($n = 6–8$). *, $p < 0.05$ compared with control; #, $p < 0.05$ compared with *db/db* MSC treatment.

the DMEM control (Fig. 5, *A* and *B*). The administration of *db/db* MSCs and 14*S*,21*R*-diHDHA together to the wounds of *db/db* mice increased wound vascularity by 205.0%, which was significantly more than the summation of the enhancement percentages by *db/db* MSCs alone (78.5%) (Fig. 5*B*) and 14*S*,21*R*-diHDHA alone (41.9%) (Fig. 2*B*), indicating a synergic effect. Therefore, 14*S*,21*R*-diHDHA remedies diabetes-impaired MSC functions and acts synergistically with MSCs to promote vascularization or angiogenesis in wounds of *db/db* mice. The synergistic promoting effect of 14*S*,21*R*-diHDHA and *db*/+ MSCs on angiogenesis was also obtained on *db*/+ mice (supplemental Fig. S5).

Endothelial cell migration and vasculature formation, the key cellular processes of angiogenesis were studied under simulated hyperglycemia to delineate the action of 14*S*,21*R*-diHDHA on diabetes-impaired angiogenic functions of *db/db* MSCs (Fig. 5, *C–F*). High glucose (25 nM) MSC-conditioned media were prepared by culturing *db/db* MSCs in the presence or absence of 14*S*,21*R*-diHDHA and by culturing *db*/+ MSCs in the absence of 14*S*,21*R*-diHDHA. The media were used to assess *db/db* DMVEC migration and vasculature formation (Fig. 5, *C–F*). Media conditioned by MSCs from *db/db* and *db*/+ mice increased *db/db* DMVEC migration 32.0 and 81.6%, respectively, and enhanced vasculature formation 43.4 and 83.3%, respectively, compared with controls (*i.e.* without MSC-conditioned media) (Fig. 5, *C–F*). As expected, medium from *db/db* MSCs without 14*S*,21*R*-diHDHA treatment exhibited significantly less *db/db* DMVEC migration and vascu-

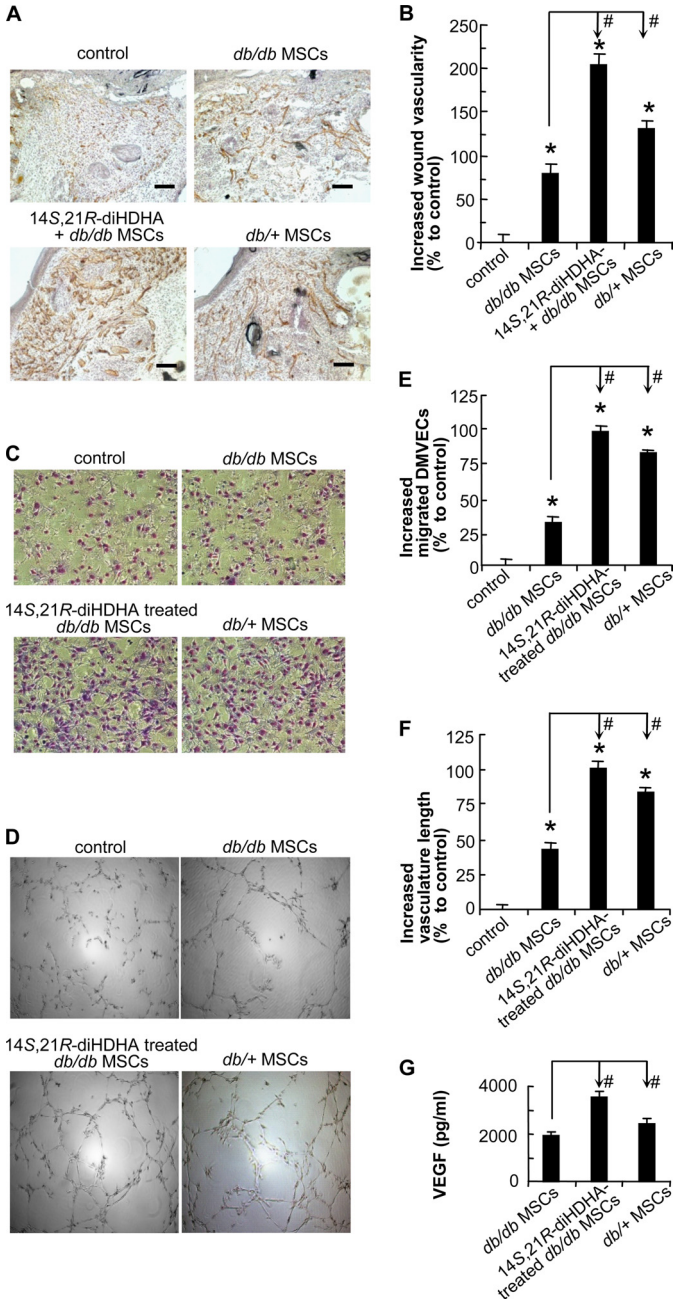

FIGURE 5. **14*S*,21*R*-diHDHA remedied impaired functions of *db/db* MSCs and acted synergistically with them in promoting angiogenesis under hyperglycemia.** The wound healing model and treatment were conducted in *db/db* mice as in Fig. 4. *A,* representative microphotographs show the $CD31^+$ vessels in wounds treated with vehicle (control), *db/db* MSCs, *db/db* MSCs plus 14*S*,21*R*-diHDHA, or *db*/+ MSCs (14*S*,21*R*-diHDHA, 50 ng/wound; MSCs, 10^6 cells/wound). *B,* increased percentages of wound vascularity compared with the control that possessed 4.4 ± 0.4% vascularity ($n = 12$). *Scale bar,* 100 μm. Cellular processes of angiogenesis were studied *in vitro* as in Fig. 3. Representative images of *db/db* DMVEC migration (*C*) and vasculature formation (*D*) are shown. The *db/db* DMVECs were studied under simulated hyperglycemia (25 mM glucose) in DMEM (control), DMEM conditioned by *db/db* MSCs with (14*S*,21*R*-diHDHA-treated *db/db* MSCs) or without (*db/db* MSCs) 14*S*,21*R*-diHDHA treatment, as well as DMEM conditioned by *db*/+ MSCs (*db*/+ MSCs). Migration (*E*) and vasculature formation (*F*) were quantified as increased percentages of migrated DMVECs per field ($n = 15$) and of vasculature length per field ($n = 4$), respectively, compared with the controls (migrated DMVECs, 118.0 ± 2.8 cells/field; vasculature length, 7.2 ± 0.3 mm/field). *G,* VEGF secretion was assayed by Bio-Plex protein array ($n = 3$). The medium was conditioned with 3×10^5 *db/db* MSCs, 14*S*,21*R*-diHDHA-treated *db/db* MSCs, or *db*/+ MSCs. Results are means ± S.E. *, $p < 0.05$ compared with control; #, $p < 0.05$ compared with *db/db* MSC treatment.

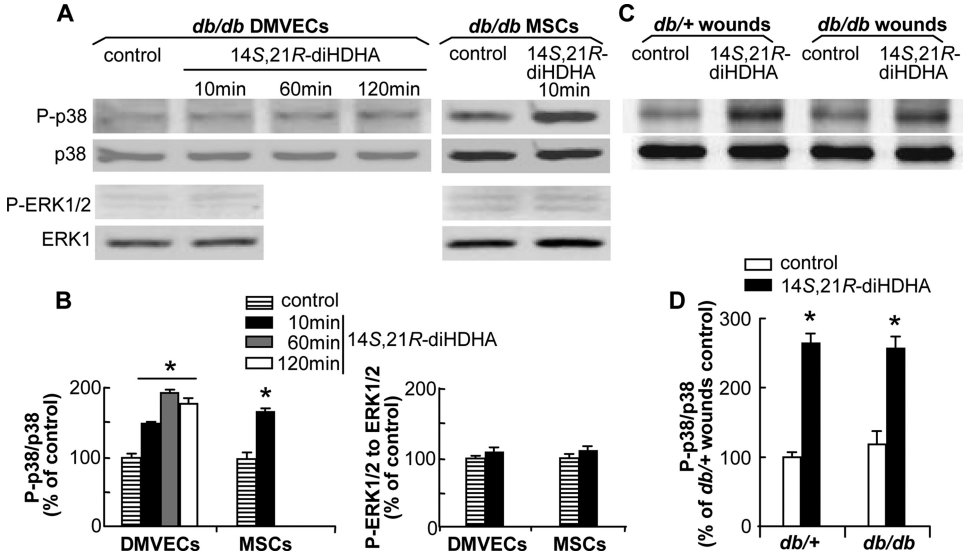

FIGURE 6. **14*S*,21*R*-diHDHA activated p38 MAPK but not ERK1/2 signaling pathway.** Quiescent subconfluent *db/db* DMVECs and MSCs were treated with 100 nM 14*S*,21*R*-diHDHA for 10–120 min, and wounds of *db/+* and *db/db* mice were treated with 14*S*,21*R*-diHDHA (50 ng/wound) for 15 min. Whole tissue and cell lysates were analyzed by Western blot with antibodies specific to phospho-p38 (P-p38) and phospho-ERK1/2 (P-ERK1/2) as well as total p38 and ERK1. Densitometric ratios of P-p38 to p38 and P-ERK1/2 to ERK1 are presented as a percentage of control (*i.e.* without 14*S*,21*R*-diHDHA treatment). Representative Western blot images of P-p38, p38, P-ERK1/2, and ERK1 as well as densitometric ratios of P-p38 to p38 and P-ERK1/2 to ERK1 in *db/db* DMVECs and MSCs (*A* and *B*), and in wounds of *db/+* and *db/db* mice (*C* and *D*) are shown. Results are mean ± S.E. ($n = 3$). *, $p < 0.05$ compared with control.

lature formation compared with *db/+* MSCs, demonstrating impaired angiogenesis. When the medium from 14*S*,21*R*-diHDHA-treated *db/db* MSCs was used, *db/db* DMVEC migration and vasculature formation were enhanced 98.5 and 101.7%, respectively, relative to the vehicle control (Fig. 5, *C–F*). These results were greater than the combined increased percentages induced by *db/db* MSCs alone (32.0% for migration and 43.4% for vasculature formation) (Fig. 5, *C–F*) and 14*S*,21*R*-diHDHA alone (45.5% for migration and 40.8% for vasculature formation) (Fig. 3, *A* and *B*). These data indicate that 14*S*,21*R*-diHDHA rescues the impaired angiogenic functions of *db/db* MSCs in promotion of DMVEC migration and vasculature formation.

MSCs secrete angiogenic cytokines such as VEGF to promote angiogenesis (22). As such, we hypothesized that 14*S*,21*R*-diHDHA promoted angiogenic functions of *db/db* MSCs partly as a result of increased angiogenic cytokine production by the cells. To test this, VEGF levels were quantified in media from *db/db* MSCs, 14*S*,21*R*-diHDHA-treated *db/db* MSCs, and *db/+* MSCs. The data demonstrate that greater amounts of VEGF were released by *db/+* MSCs than that by *db/db* MSCs (Fig. 5*G*), consistent with impaired angiogenesis in *db/db* MSCs. This impairment was restored by 14*S*,21*R*-diHDHA treatment, which induced *db/db* MSCs to secrete significantly more VEGF under simulated hyperglycemia (Fig. 5*G*). Taken together, these results suggest that 14*S*,21*R*-diHDHA can rescue the functions of *db/db* MSCs or synergize with *db/db* MSCs to promote angiogenesis by rescuing *db/db* MSC paracrine angiogenic functions.

14S,21R-diHDHA Activates the p38 but Not ERK1/2 Signaling Pathway—Activation of MAPK pathways is essential in wound healing and associated angiogenesis (28, 48, 49). Therefore, we sought to determine whether 14*S*,21*R*-diHDHA treatment led to activation of the MAPKs. Our results showed that 14*S*,21*R*-diHDHA treatment triggered phosphorylation of p38 in *db/db* DMVECs and MSCs, but had no effect on phosphorylation of ERK1/2. The ratio of phosphorylated to nonphosphorylated p38 in *db/db* DMVECs treated with 14*S*,21*R*-diHDHA remained higher than that of the control for at least 120 min (Fig. 6, *A* and *B*). In addition, 14*S*,21*R*-diHDHA treatment increased the levels of phosphorylated p38 in wounds of *db/+* and *db/db* mice, and there was no significantly different levels of phosphorylated p38 in wounds of *db/+* and *db/db* mice (Fig. 6, *C* and *D*).

DISCUSSION

The reduced formation of the novel reparative lipid mediator, 14*S*,21*R*-diHDHA, in cutaneous wounds of *db/db* diabetic mice indicates that diabetes suppresses the formation of this molecule (Fig. 1). Platelet (P)12-LOX, the enzyme counted for 12-LOX-activity of platelets (31, 50, 51), or L-12-LOX (5) converts DHA to 14*S*-hydroperoxy-DHA (14*S*-hydroperoxy-DHA), which is reduced to 14*S*-HDHA in tissues and further transformed to 14*S*,21*R*-diHDHA by the P450 enzyme (11). The formation of 14*S*-HDHA, the intermediate in 14*S*,21*R*-diHDHA biosynthetic pathways and a marker of 12-LOX activity (11), was also modestly reduced in diabetic wounds (Fig. 1*B, middle panel*). These results indicate that critical 12-LOX-related 14*S*-hydroxylation for biosynthesis of 14*S*,21*R*-diHDHA in wounds could be impaired in diabetes. The hyperglycemia and excessive oxidative stress in diabetic wounds appears to have impaired the DHA 14*S*-hydroxylation system, which reduced 14*S*,21*R*-diHDHA formation (Scheme 1).

It has been reported that the knock-out of 12/15(or L-12)LOX gene from mice reduced DHA 14-hydroxylation by peritoneal macrophages by >95% (5). There was no report before to study of the effect of 12/15-LOX knock-out on DHA

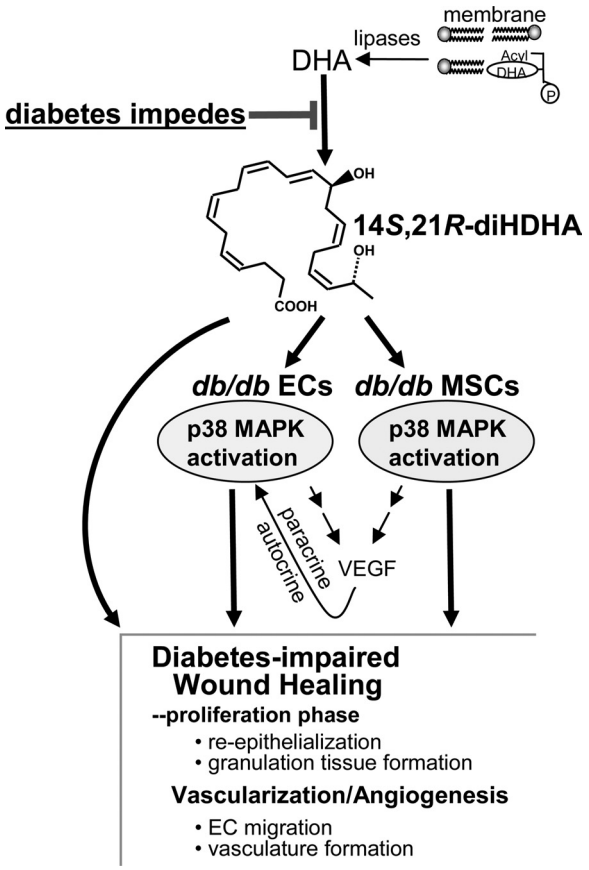

SCHEME 1. **Diabetes reduces formation of 14*S*,21*R*-diHDHA in cutaneous wounds and application of exogenous 14*S*,21*R*-diHDHA counteracts the diabetic impairment on healing, angiogenesis, and associated functions of mesenchymal stem cells.** Treatment with 14*S*,21*R*-diHDHA rescues healing, angiogenesis, and associated MSC functions that are impaired in diabetes. 14*S*,21*R*-diHDHA restores the diabetes-impaired cellular processes of angiogenesis and paracrine functions of MSCs, including endothelial cell (*EC*) migration, vasculature formation, and production of VEGF (autocrine and paracrine). This lipid mediator activates the p38 MAPK pathway in endothelial cells and MSCs. 14*S*,21*R*-diHDHA may also act directly to enhance re-epithelialization and granulation tissue formation in wound healing.

14-hydroxylation in skin. Our results showed that 12/15-LOX knock-out reduced the formation of 14*S*-HDHA and 14*S*,21*R*-diHDHA in the murine skin wounds (Fig. 1*B*). The portion of 14*S*-HDHA that was still formed in 12/15-LOX-KO skin may result from P-12-LOX which is known to efficiently participate DHA 14*S*-hydroxylation and exist in murine skin (51–53). Therefore, L-12-LOX plays a role in producing 14*S*,21*R*-diHDHA in skin wounds (Fig. 1). Additionally P-12-LOX is likely to participate in DHA 14*S*-hydroxylation. The levels of 14*S*-HDHA and 14*S*,21*R*-diHDHA in the skin wounds of *db/+* mice were quite different from those of C57BL/6 mice (Fig. 1*B*), which may be due to the distinct phenotypic difference between two strains (strain information, The Jackson Laboratory).

In murine skin wounds, there are other lipoxygenases, including epidermis-type LOX3, 12*R*-LOX, and 8-LOX as well as 5-LOX from recruited leukocytes (26, 30, 31, 50, 53–59). However, LOX3, 12*R*-LOX, 8-LOX, or 5-LOX is unlikely to catalyze DHA 14*S*-hydroxygenation in skin wounds based on the study conducted by other scientists (52) and ourselves.[3] Therefore, L- and P-12-LOXs could be the major 12-LOXs responsible in 14*S*-hydroxylation for 14*S*,21*R*-diHDHA formation. Diabetes could affect L- and/or P-12-LOX in skin wounds, which is of our interest for future study.

21-Hydroxyl in 14,21-diHDHAs is a ϖ-1-hydroxyl, thus it is very likely to be generated by specific P450, such as 2E1 (60) or other P450s. P450 CYP1A1, 2B6/7, 2E1, 3A4/7, and 3A5 were identified at protein level and found to possess catalytic activities in skin (61); and many other P450s were found in skin at mRNA level (61). It is known that CYP2E1 generates 19-hydroxyleicosatetraenoic acid, an ϖ-1 hydroxylation product from arachidonic acid substrate (60); therefore, it is likely to participate in the ϖ-1 hydroxylation of 14*S*-HDHA substrate for the formation of 14*S*,21*R*-diHDHA in the skin (60).

Moreover, treating wounds with 14*S*,21*R*-diHDHA improved healing as well as vascularization or angiogenesis in diabetic mice (Fig. 2). Treatment with 14*S*,21*R*-diHDHA also rescued the key cellular processes of healing-associated angiogenesis: DMVEC transmigration and vasculature formation (Fig. 3). Angiogenesis is critical for growing new vessels that are essential for optimal healing (1). Endothelial cells in the vascular network adjacent to wounds migrate, proliferate, and undergo vascularization and neovessel formation within the granulation tissue (62). Diabetes impairs angiogenesis and causes microcirculatory deficiencies in skin wounds (1, 2). Thus, new approaches toward ameliorating impaired angiogenesis would significantly contribute to efforts to develop better treatments for diabetic wounds (2, 63). 14*S*,21*R*-diHDHA represents a new lead for this approach. The promotion of re-epithelialization and granulation tissue formation by 14*S*,21*R*-diHDHA in wounds suggests that this lipid mediator may also enhance other cellular processes of healing that involve epithelial cells and fibroblast cells (Scheme 1) (64).

When 14*S*,21*R*-diHDHA was combined with *db/db* MSCs and used to treat the wounds of diabetic *db/db* mice, the combination promoted the crucial processes of wound healing: re-epithelialization and granulation tissue growth (Figs. 2 and 4) (34, 65). Furthermore, 14*S*,21*R*-diHDHA was observed to restore diabetes-impaired angiogenic functions of *db/db* MSCs that promote wound vascularization, as well as *db/db* DMVEC migration and vasculature formation (Figs. 3 and 5). 14*S*,21*R*-diHDHA stimulated *db/db* DMVECs (Fig. 3*C*) and MSCs to increase VEGF secretion (Fig. 5*G*), which is at least partly responsible for accelerated angiogenesis in wound healing (Scheme 1). VEGF is one of the most important angiogenic cytokines (48) and promotes wound healing through enhancing angiogenesis (63). By producing VEGF, DMVECs promote their own angiogenesis processes, and MSCs promote vascularization achieved by endothelial cells and other type cells in wounds; thus DMVECs and MSCs manifest their autocrine and/or paracrine functions of promoting angiogenesis in wound healing (Scheme 1). The promotion of VEGF production represents a molecular mechanism for the pro-angiogenic functions of 14*S*,21*R*-diHDHA in wound healing

[3] H. Tian, Y. Lu, S. P. Shah, and S. Hong, unpublished data.

and also further indicates that 14*S*,21*R*-diHDHA remedies diabetes-impaired pro-angiogenic functions of *db/db* MSCs.

Treatment of nonhealing wounds in diabetic patients with autologous MSCs is of clinical significance, but its value is restricted by deficient functions of the MSCs due to diabetes. In this regard, being a remedy for diabetes-impaired pro-healing functions of *db/db* MSCs, 14*S*,21*R*-diHDHA is a promising new compound that could clinically restore these impaired MSC functions.

Activation of p38 and/or ERK1/2 is required for normal angiogenesis (27), including endothelial cell migration and vasculature formation (49, 66). p38 and ERK1/2 activation also have important roles in VEGF expression in endothelial cells and MSCs (67, 68). 14*S*,21*R*-diHDHA treatment results in immediate phosphorylation of p38 in wounds, *db/db* DMVECs, and MSCs, but not of ERK1/2, in *db/db* DMVECs and MSCs (Fig. 6), which suggests that the p38 signaling pathway is involved in 14*S*,21*R*-diHDHA promotion of healing and angiogenesis in diabetic wounds and MSC angiogenic functions. The receptor(s) of 14*S*,21*R*-diHDHA and mechanisms for 14*S*,21*R*-diHDHA activation of p38 signaling pathways are of interest for our future studies.

As summarized in Scheme 1, our studies reveal that diabetes impedes the formation of 14*S*,21*R*-diHDHA in wounds. Administration of exogenous 14*S*,21*R*-diHDHA rescues diabetes-impaired healing, angiogenesis, and associated MSC functions. These actions of 14*S*,21*R*-diHDHA appear to involve the activation of p38-MAPK signaling in endothelial cells and MSCs. This study identifies the novel lipid mediator, 14*S*,21*R*-diHDHA, as an important new lead for developing better therapeutics in the treatment of diabetic wounds.

The supplemental Fig. S1 shows the detailed isolation and identification of DMVECs and MSCs from mice. The supplemental Fig. S2 demonstrated that 14*S*,21*R*-diHDHA generated from 14*S*-HDHA by h-P450 and separated by chiral LC is highly pure, confirmed its structure by LC-MS/MS analysis of its hydrogenated product, and further justified its chiral analysis using the analogous diastereomers. The supplemental Fig. S3 shows that several products are generated by h-P450 from 14*S*-HDHA and are separated from 14*S*,21*R*-diHDHA by the chiral LC. The supplemental Fig. S4 shows 14*S*,21*R*-diHDHA coacts with *db/+* MSCs to promote wound healings in *db/+* mice. The supplemental Fig. S5 shows the synergistic effect of 14*S*,21*R*-diHDHA and *db/+* MSCs on angiogenesis in *db/+* mice. The supplemental Fig. S6 shows 14*S*,21*R*-diHDHA improves the cellular angiogenic processes of *db/+* DMVECs.

Acknowledgments—We are very grateful to Dr. Nicolas Bazan (Neuroscience Center of Excellence at Louisiana State University Health Sciences Center) and Dr. Charles N. Serhan (Brigham and Women's Hospital, Harvard Medical School) for providing authentic synthetic standards of protectin/neuroprotectin D1 and its isomers. We thank Ryan R. Labaden and Dr. Eric C. B. Milner for their expertise in editing and manuscript preparation, and we thank Dr. Ping Zhang and Constance Porretta (Louisiana State University Health Sciences Center Immunology Core) for FACS analysis.

REFERENCES

1. Falanga, V. (2005) *Lancet* **366,** 1736–1743
2. Javazon, E. H., Keswani, S. G., Badillo, A. T., Crombleholme, T. M., Zoltick, P. W., Radu, A. P., Kozin, E. D., Beggs, K., Malik, A. A., and Flake, A. W. (2007) *Wound Repair Regen.* **15,** 350–359
3. Montori, V. M., Farmer, A., Wollan, P. C., and Dinneen, S. F. (2000) *Diabetes Care* **23,** 1407–1415
4. Shingel, K. I., Faure, M. P., Azoulay, L., Roberge, C., and Deckelbaum, R. J. (2008) *J. Tissue Eng. Regen. Med.* **2,** 383–393
5. Serhan, C. N., Yang, R., Martinod, K., Kasuga, K., Pillai, P. S., Porter, T. F., Oh, S. F., and Spite, M. (2009) *J. Exp. Med.* **206,** 15–23
6. Serhan, C. N., Clish, C. B., Brannon, J., Colgan, S. P., Chiang, N., and Gronert, K. (2000) *J. Exp. Med.* **192,** 1197–1204
7. Serhan, C. N., Hong, S., Gronert, K., Colgan, S. P., Devchand, P. R., Mirick, G., and Moussignac, R. L. (2002) *J. Exp. Med.* **196,** 1025–1037
8. Hong, S., Gronert, K., Devchand, P. R., Moussignac, R. L., and Serhan, C. N. (2003) *J. Biol. Chem.* **278,** 14677–14687
9. Marcheselli, V. L., Hong, S., Lukiw, W. J., Tian, X. H., Gronert, K., Musto, A., Hardy, M., Gimenez, J. M., Chiang, N., Serhan, C. N., and Bazan, N. G. (2003) *J. Biol. Chem.* **278,** 43807–43817
10. Gronert, K., Maheshwari, N., Khan, N., Hassan, I. R., Dunn, M., and Laniado Schwartzman, M. (2005) *J. Biol. Chem.* **280,** 15267–15278
11. Lu, Y., Tian, H., and Hong, S. (2010) *J. Lipid Res.* **51,** 923–932
12. Brownlee, M. (2001) *Nature* **414,** 813–820
13. Schäfer, M., and Werner, S. (2008) *Pharmacol. Res.* **58,** 165–171
14. Kämpfer, H., Schmidt, R., Geisslinger, G., Pfeilschifter, J., and Frank, S. (2005) *Diabetes* **54,** 1543–1551
15. Kapoor, M., Kojima, F., Appleton, I., Kawai, S., and Crofford, L. J. (2006) *Curr. Opin. Investig. Drugs* **7,** 418–422
16. Jiang, Y., Jahagirdar, B. N., Reinhardt, R. L., Schwartz, R. E., Keene, C. D., Ortiz-Gonzalez, X. R., Reyes, M., Lenvik, T., Lund, T., Blackstad, M., Du, J., Aldrich, S., Lisberg, A., Low, W. C., Largaespada, D. A., and Verfaillie, C. M. (2002) *Nature* **418,** 41–49
17. Liu, J. W., Dunoyer-Geindre, S., Serre-Beinier, V., Mai, G., Lambert, J. F., Fish, R. J., Pernod, G., Buehler, L., Bounameaux, H., and Kruithof, E. K. (2007) *J. Thromb. Haemost.* **5,** 826–834
18. Wang, X., Hisha, H., Taketani, S., Adachi, Y., Li, Q., Cui, W., Cui, Y., Wang, J., Song, C., Mizokami, T., Okazaki, S., Li, Q., Fan, T., Fan, H., Lian, Z., Gershwin, M. E., and Ikehara, S. (2006) *Stem Cells* **24,** 482–493
19. Wu, Y., Chen, L., Scott, P. G., and Tredget, E. E. (2007) *Stem Cells* **25,** 2648–2659
20. Lin, C. D., Allori, A. C., Macklin, J. E., Sailon, A. M., Tanaka, R., Levine, J. P., Saadeh, P. B., and Warren, S. M. (2008) *Plast. Reconstr. Surg.* **122,** 1341–1351
21. Kwon, D. S., Gao, X., Liu, Y. B., Dulchavsky, D. S., Danyluk, A. L., Bansal, M., Chopp, M., McIntosh, K., Arbab, A. S., Dulchavsky, S. A., and Gautam, S. C. (2008) *Int. Wound J.* **5,** 453–463
22. Chen, L., Tredget, E. E., Wu, P. Y., and Wu, Y. (2008) *PLoS ONE* **3,** e1886
23. Broughton, G., 2nd, Janis, J. E., and Attinger, C. E. (2006) *Plast. Reconstr. Surg.* **117,** 12S–34S
24. Stepanovic, V., Awad, O., Jiao, C., Dunnwald, M., and Schatteman, G. C. (2003) *Circ. Res.* **92,** 1247–1253
25. Han, X. (2007) *Curr. Opin. Mol. Ther.* **9,** 586–591
26. Sun, D., and Funk, C. D. (1996) *J. Biol. Chem.* **271,** 24055–24062
27. Gee, E., Milkiewicz, M., and Haas, T. L. (2010) *J. Cell. Physiol.* **222,** 120–126
28. Sharma, G. D., He, J., and Bazan, H. E. (2003) *J. Biol. Chem.* **278,** 21989–21997
29. Cyrus, T., Witztum, J. L., Rader, D. J., Tangirala, R., Fazio, S., Linton, M. F., and Funk, C. D. (1999) *J. Clin. Invest.* **103,** 1597–1604
30. Funk, C. D. (2001) *Science* **294,** 1871–1875
31. Funk, C. D., Chen, X. S., Johnson, E. N., and Zhao, L. (2002) *Prostaglandins Other Lipid Mediat.* **68–69,** 303–312
32. Klein, R. F., Allard, J., Avnur, Z., Nikolcheva, T., Rotstein, D., Carlos, A. S., Shea, M., Waters, R. V., Belknap, J. K., Peltz, G., and Orwoll, E. S. (2004) *Science* **303,** 229–232

33. Cha, S. T., Talavera, D., Demir, E., Nath, A. K., and Sierra-Honigmann, M. R. (2005) *Microvasc. Res.* **70,** 198–204
34. Galiano, R. D., Michaels, J., 5th., Dobryansky, M., Levine, J. P., and Gurtner, G. C. (2004) *Wound Repair Regen.* **12,** 485–492
35. Basselin, M., Kim, H. W., Chen, M., Ma, K., Rapoport, S. I., Murphy, R. C., and Farias, S. E. (2010) *J. Lipid Res.* **51,** 1049–1056
36. Yang, P., Chan, D., Felix, E., Madden, T., Klein, R. D., Shureiqi, I., Chen, X., Dannenberg, A. J., and Newman, R. A. (2006) *Prostaglandins Leukot. Essent. Fatty Acids* **75,** 385–395
37. Gronert, K., Clish, C. B., Romano, M., and Serhan, C. N. (1999) *Methods Mol. Biol.* **120,** 119–144
38. Bazan, N. G., Marcheselli, V. L., Lu, Y., Hong, S., and Jackson, F. (2008) in *Signal Transduction in the Retina* (Fliesler, S. J., and Kisselev, O. G., eds) pp. 345–374, CRC Press, Inc., Boca Raton, FL
39. Hall, L. M., and Murphy, R. C. (1998) *J. Am. Soc. Mass Spectrom.* **9,** 527–532
40. Schneider, C., Yu, Z., Boeglin, W. E., Zheng, Y., and Brash, A. R. (2007) *Methods Enzymol.* **433,** 145–157
41. Schwenk, U., Morita, E., Engel, R., and Schröder, J. M. (1992) *J. Biol. Chem.* **267,** 12482–12488
42. Marcus, A. J., Safier, L. B., Ullman, H. L., Broekman, M. J., Islam, N., Oglesby, T. D., and Gorman, R. R. (1984) *Proc. Natl. Acad. Sci. U.S.A.* **81,** 903–907
43. Steffenrud, S., Borgeat, P., Evans, M. J., and Bertrand, M. J. (1987) *Biomed. Environ. Mass Spectrom.* **14,** 313–323
44. Serhan, C. N., Gotlinger, K., Hong, S., Lu, Y., Siegelman, J., Baer, T., Yang, R., Colgan, S. P., and Petasis, N. A. (2006) *J. Immunol.* **176,** 1848–1859
45. Colville-Nash, P. R., and Willoughby, D. A. (1997) *Mol. Med. Today* **3,** 14–23
46. Adler, A. I., Boyko, E. J., Ahroni, J. H., and Smith, D. G. (1999) *Diabetes Care* **22,** 1029–1035
47. Ding, Y., Vaziri, N. D., Coulson, R., Kamanna, V. S., and Roh, D. D. (2000) *Am. J. Physiol. Endocrinol. Metab.* **279,** E11–E17
48. Li, J., Zhang, Y. P., and Kirsner, R. S. (2003) *Microsc. Res. Tech.* **60,** 107–114
49. Bajpai, A. K., Blaskova, E., Pakala, S. B., Zhao, T., Glasgow, W. C., Penn, J. S., Johnson, D. A., and Rao, G. N. (2007) *Invest. Ophthalmol. Vis. Sci.* **48,** 4930–4938
50. Fürstenberger, G., Epp, N., Eckl, K. M., Hennies, H. C., Jørgensen, C., Hallenborg, P., Kristiansen, K., and Krieg, P. (2007) *Prostaglandins Other Lipid Mediat.* **82,** 128–134
51. Kim, H. Y., Karanian, J. W., Shingu, T., and Salem, N., Jr. (1990) *Prostaglandins* **40,** 473–490
52. Siebert, M., Krieg, P., Lehmann, W. D., Marks, F., and Fürstenberger, G. (2001) *Biochem. J.* **355,** 97–104
53. Johnson, E. N., Nanney, L. B., Virmani, J., Lawson, J. A., and Funk, C. D. (1999) *J. Invest. Dermatol.* **112,** 861–865
54. Chen, X. S., Kurre, U., Jenkins, N. A., Copeland, N. G., and Funk, C. D. (1994) *J. Biol. Chem.* **269,** 13979–13987
55. Boeglin, W. E., Kim, R. B., and Brash, A. R. (1998) *Proc. Natl. Acad. Sci. U.S.A.* **95,** 6744–6749
56. Moran, J. L., Qiu, H., Turbe-Doan, A., Yun, Y., Boeglin, W. E., Brash, A. R., and Beier, D. R. (2007) *J. Invest. Dermatol.* **127,** 1893–1897
57. Epp, N., Fürstenberger, G., Müller, K., de Juanes, S., Leitges, M., Hausser, I., Thieme, F., Liebisch, G., Schmitz, G., and Krieg, P. (2007) *J. Cell Biol.* **177,** 173–182
58. Yu, Z., Schneider, C., Boeglin, W. E., and Brash, A. R. (2006) *Arch. Biochem. Biophys.* **455,** 188–196
59. Krieg, P., Kinzig, A., Heidt, M., Marks, F., and Fürstenberger, G. (1998) *Biochim. Biophys. Acta* **1391,** 7–12
60. Laethem, R. M., Balazy, M., Falck, J. R., Laethem, C. L., and Koop, D. R. (1993) *J. Biol. Chem.* **268,** 12912–12918
61. Swanson, H. I. (2004) *Chem. Biol. Interact.* **149,** 69–79
62. Velazquez, O. C. (2007) *J. Vasc. Surg.* **45,** Suppl. A, 39–47
63. Galiano, R. D., Tepper, O. M., Pelo, C. R., Bhatt, K. A., Callaghan, M., Bastidas, N., Bunting, S., Steinmetz, H. G., and Gurtner, G. C. (2004) *Am. J. Pathol.* **164,** 1935–1947
64. Martin, P., and Leibovich, S. J. (2005) *Trends Cell Biol.* **15,** 599–607
65. Braiman-Wiksman, L., Solomonik, I., Spira, R., and Tennenbaum, T. (2007) *Toxicol. Pathol.* **35,** 767–779
66. Huang, Q., and Sheibani, N. (2008) *Am. J. Physiol. Cell Physiol.* **295,** C1647–C1657
67. Mezentsev, A., Seta, F., Dunn, M. W., Ono, N., Falck, J. R., and Laniado-Schwartzman, M. (2002) *J. Biol. Chem.* **277,** 18670–18676
68. Kim, I. S., Song, J. K., Song, Y. M., Cho, T. H., Lee, T. H., Lim, S. S., Kim, S. J., and Hwang, S. J. (2009) *Tissue Eng. Part A* **15,** 2411–2422